Full Paper: Polyolefine elastomers with varying 1-octene content and different thermal history are studied by wide–angle X-ray scattering (WAXS) and small–angle X-ray scattering (SAXS) during drawing and after relaxation. The multidimensional chord distribution function (CDF) reveals the nanostructure made from crystallites in the amorphous matrix. Both lamellae and granular crystals are found. Lamellae do not form stacks. The SAXS peak is observed because each lamella is covered by an amorphous layer of well–defined thickness. Arrangement, rotation, fine chain slip and failure of the domains are directly observed as a function of elongation. During straining and relaxation a well oriented macrolattice with colloidal dimensions but short–ranging order is formed. Two processes are generating microfibrils, namely (1) arrangement of granular crystallites, and (2) irreversible disruption of lamellae (coarse slip) followed by arrangement of their fragments. The second process stabilizes the colloidal lattice permanently. The higher the comonomer content, the later the irreversible process starts. Quenching from the melt shifts the onset to lower deformation. Deformation of microfibrils is not homogeneous. Instead, there is a limiting long period that cannot be exceeded without disruption. It is related to the position of the maximum in the SAXS pattern (which is almost constant).

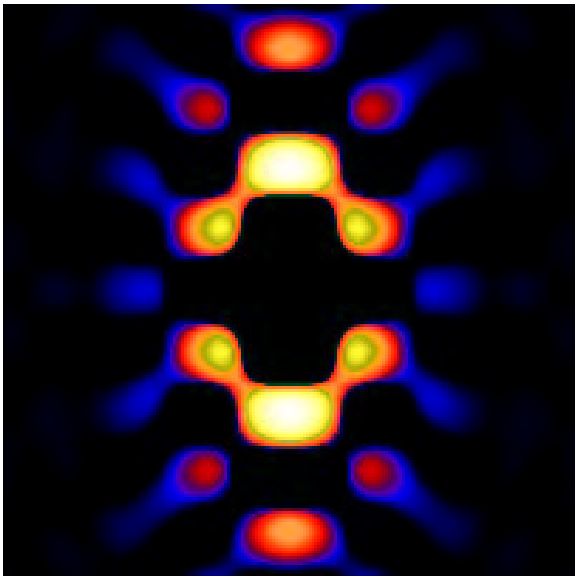

Long periods in the CDF $z\left(r_{12}, r_3\right)$ of an ethylene-octene block copolymer after relaxation from drawing

Nanostructure Evolution of Homogeneous Poly(ethylene-*co*-1-octene) as a Function of Strain

Norbert Stribeck[1]*, *René Androsch*[2], *Sérgio S. Funari*[3]

[1] University of Hamburg, Institute of Technical and Macromolecular Chemistry, Bundesstr. 45, 20146 Hamburg, Germany. FAX:+49-40-42838-6008; E-mail: Norbert.Stribeck@desy.de
[2] Martin Luther University Halle Wittenberg, Institute of Materials Science, 06217 Merseburg, Germany
[3] Max Planck Institute of Colloids and Interfaces, c/o HASYLAB, 22603 Hamburg, Germany

Keywords: drawing; elastomers; nanostructures; SAXS; thermoplastics;

Introduction

Homogeneous copolymers of ethylene and α–olefines form a broad range of semicrystalline nanostructures. They range from highly crystalline, lamellar morphologies known for polyethylene homopolymer to a granular morphology of low crystallinity copolymers. The materials became available on a large scale after the industrial implementation of metallocene catalysis in the 1990s. Sometimes they are addressed as linear low density polyethylene (LLDPE).[1]

The chemical microstructure of these copolymers differs significantly from that of conventional linear polyethylene. The molecular weight distribution is narrow, and the comonomer distribution is homogeneous. Thus the chemical microstructure is well–defined, and it is not astonishing that the availability of these materials has contributed to a wave of fundamental studies in the field concerning the melting and crystallization of polymers. Of similar scientific interest are investigations which are aiming at understanding the broad range of materials properties covered by these copolymers.

Ultimately, both classes of problems result in the quest to elucidate the nanostructure evolution as a function of load

— thermal in the first, and mechanical in the second case. For such studies imaging methods are of limited use, and small–angle scattering is a method of choice. The power of this method rests both upon the design of brilliant (synchrotron) radiation sources and on progress in the fields of scattering theory and data analysis. Published papers indicate the progress of radiation sources, but a considerable backlog where the advance of data analysis method is concerned. Here we put forward an investigation utilizing the method of multidimensional chord distribution function (CDF) analysis[2] and demonstrate its power concerning the description of nanostructure evolution processes.

According to Bensason et al.,[3] ethylene-octene copolymers are classified by four distinct categories. Transmission electron microscopy (TEM) images of the corresponding nanostructures at ambient temperature have been published by Chen et al.[4] The samples of the present study belong to the low crystallinity categories of Type I (granular, non-lamellar morphology) and Type II (mixed morphology of small lamellae and bundled crystals). Under mechanical load the materials exhibit homogeneous straining behavior, and features of both elastomeric and plastic deformation.[5] Following the notions of Peterlin,[6,7] tensile failure modes related to the load–elongation behavior of the materials are both discussed on a molecular level and on the colloidal or nanodomain scale. On the molecular level three processes are addressed as: fine chain slip (going along with crystallite thinning), coarse chain slip (going along with crystallite disruption), and chain scission.[6,8–14] On the nanodomain scale reversible processes of interlamellar deformation and lamellar thinning[10] are discussed to be followed by irreversible microfibrillation.[6]

Butler et al.[11,15] study LLDPE during straining by small–angle X–ray scattering (SAXS) in the synchrotron beam both in comparison to high–density polyethylene, and as a function of different comonomers.[10] They compare SAXS and WAXS patterns to the stress–strain curves and find that microfibrillation occurs immediately after a second yield point as the load drops. Related to the plateau of the curves, deformation of microfibrils is detected. One of us (Androsch et al.[16]) has studied ethylene–octene copolymers with low comonomer content and corresponding lamellar nanostructure as a function of mechanical load. Lamellar stacks with their axes becoming oriented perpendicular to the draw direction are reported. A preceding paper[17] reports changes of the SAXS and WAXS patterns and discusses them in comparison with results from tensile tests and differential scanning calorimetry.

In the present study we extract the information concerning the semicrystalline nanostructure from the scattering patterns and utilize the multidimensional chord distribution function (CDF) to display and discuss the domain structure in physical space. We proceed in wider intervals of strain, up to the regime of classical fibrillation.[7] In this way we avoid having to deal with any imperfect orientation of crystallites observed at low elongations, and with the related problem of separating the orientation distribution from the local nanostructure.

Experimental Part

Materials

INSITE® homogeneous poly(ethylene-*co*-1-octene) copolymers containing different fractions of 1-octene were provided by The Dow Chemical Company. Material designation, density and 1-octene content are reported in Table 1.

Table 1: Poly(ethylene-*co*-1-octene) copolymers: Mass densities and 1-octene contents.

material designation	density $[\mathrm{g\,cm^{-3}}]$	wt–% 1-octene
EO38	0.870	38
EO30	0.885	30
EO19	0.902	19

The characterization methods have been described elsewhere.[17] From the materials, sample sheets were prepared in two different ways which are indicated by suffixes '-1' or '-q'. Films of 1 mm thickness were slowly cooled at 1 K $\mathrm{min^{-1}}$ from 463 K to 298 K ('-1'), and films of 0.5 mm were quenched in cold water after shaping in a hydraulic press ('-q'). For the study of the deformation behavior, samples of dimensions 100 mm × 15 mm were cut from the sheets.

Wide- and Small-Angle X-ray Scattering

The investigation of the sample morphology as a function of deformation was carried out at HASYLAB, Hamburg, beamline A2. Monochromatic radiation of 0.15 nm wavelength was used. Image plates were positioned at distances of 70 mm and 1780 mm from the sample for registration of the WAXS and SAXS, respectively. Exposure times were between 10 s and 20 s for registration of the WAXS, and 600 s for registration of the SAXS. The specimens were mounted in a straining stage (courtesy of B. Heise, University of Ulm, Germany), slowly (5 mm $\times\mathrm{min^{-1}}$) strained up to a chosen true elongation ε and exposed. Elongation is defined by $\varepsilon = (\ell - \ell_0)/\ell_0$, with ℓ and ℓ_0 being the actual and the initial distance between two marks on the sample, respectively. Thus patterns were taken at constant strain. X-ray patterns of

the released samples were measured, the earliest 12 h after unloading.

Valid WAXS data were recorded in an area detector of 18 cm × 18 cm. Valid SAXS data were recorded in a circular region of radius $s_r = 0.42\,\mathrm{nm}^{-1}$ in units of the scattering vector $\mathbf{s} = (s_{12}, s_3)$ with its components in cylindrical coordinates and the modulus definition $s = |\mathbf{s}| = (2/\lambda)\sin\theta$. Here λ is the wavelength of X-radiation, and 2θ is the scattering angle.

SAXS Data Evaluation

Images were normalized with respect to the incident flux and blind areas were masked. The instrument background was subtracted considering sample absorption. Center and orientation of the patterns were determined. As the final step of preprocessing, the patterns were aligned and averaged with respect to the four quadrants.

Post-processing was performed similar to the procedure described in earlier work.[2,18] Strained samples were processed to yield a three-dimensional chord distribution, $z(r_{12}, r_3)$, with cylindrical symmetry. The positions of maxima and minima in $z(r_{12}, r_3)$ were determined. Based on these data conclusions on the nanostructure were drawn.

In detail, remnant blind spots were filled in the preprocessed data utilizing two-dimensional extrapolation by radial basis functions.[19] Using the same procedure, data were extrapolated to fill the cylindrical volume $-0.5\,\mathrm{nm}^{-1} < s_{12},\, s_3 < 0.5\,\mathrm{nm}^{-1}$. The images were projected onto the fiber plane, multiplied by s^2, and a preliminary constant background was subtracted. The remnant background to be subtracted was constructed by iterative spatial frequency filtering.[2] Well-balanced interference functions of the two-phase nanostructure, $G(s_{12}, s_3)$, were obtained after three iterations. These functions finally underwent a 2D Fourier transformation, resulting in multidimensional chord distribution functions (CDFs) of the nanostructure. The interpretation of the CDF is straightforward, since it has been defined[2] by the Laplacian of Vonk's multidimensional correlation function.[20] As such, it presents the autocorrelation of the surfaces from the colloidal domains in space in a similar manner as Ruland's interface distribution function[21,22] does for one-dimensional structures as a function of distance. For samples with fiber symmetry the CDF, $z(r_{12}, r_3)$, is a function of two co-ordinates only (transverse direction, r_{12}, and fiber direction, r_3). Therefore it can be displayed by means of contours or as a density plot in the plane. Positive peaks found in the vicinity of the origin are size distributions of the primary domains. Thus their size, shape and orientation in space are depicted. Negative peaks following farther out exhibit 'long periods', i.e. the distance of two adjacent domains from each other. Positive peaks following next describe the size and orientation of superdomains (i.e. clusters made from two adjacent domains), and correlations among domains more distant are manifested in consecutive peaks at even longer distance.

Results and Discussion

Scattering Data Recorded during Straining

In preceding work[17] we have reported and discussed the orientation of anisotropic crystallites at low elongations. Now we utilize the chord distribution function (CDF) and confirm this effect. Nevertheless, as long as we are unable to separate the orientation distribution from the local nanostructure, we are unable to gain new insight concerning the orientation process itself.

Figures 1-6 show two-dimensional scattering data collected during sample straining (in vertical direction) of six samples at selected elongations ε. The sequence starts with the sample that is closest related to common polyethylene (lowest comonomer content, slowly cooled) and stops with the most different sample (highest comonomer content, quenched from the melt). Data describing the structure after relaxation is presented in the following section.

In each figure the WAXS data are documented in the first column. The pseudo color images in a logarithmic intensity scale point out the weak peaks as well. Clippings of some of these images in a linear scale are published in the earlier paper.[17] At $\varepsilon = 0$ artificial penumbra is caused from the clamps of the tensile testing machine. The original size of the displayed square is 12 cm × 12 cm, taken in a distance of 7 cm from the sample.

The second column shows sections of the preprocessed (cf. Experimental Part) SAXS images in the range $-0.25\,\mathrm{nm}^{-1} < s_{12},\, s_3 < 0.25\,\mathrm{nm}^{-1}$.

From the SAXS patterns the nanostructure information concerning the two-phase system was extracted by spatial frequency filtering and stored as the multidimensional chord distribution function (CDF). The images of the CDF in the third and fourth column of the figures depict correlations between domain interfaces for displacements of up to $\pm 50\,\mathrm{nm}$.

The third column exhibits the positive peaks from the CDF. All negative values are set equal to zero. The heights of the positive peaks are in a logarithmic scale. Here the elevations close to the origin evidence the distributions of crystalline and amorphous domains with respect to shape, size and orientation. Peaks found farther out describe the outer dimensions of 'super domains', i.e. clusters of two or more primary domains.

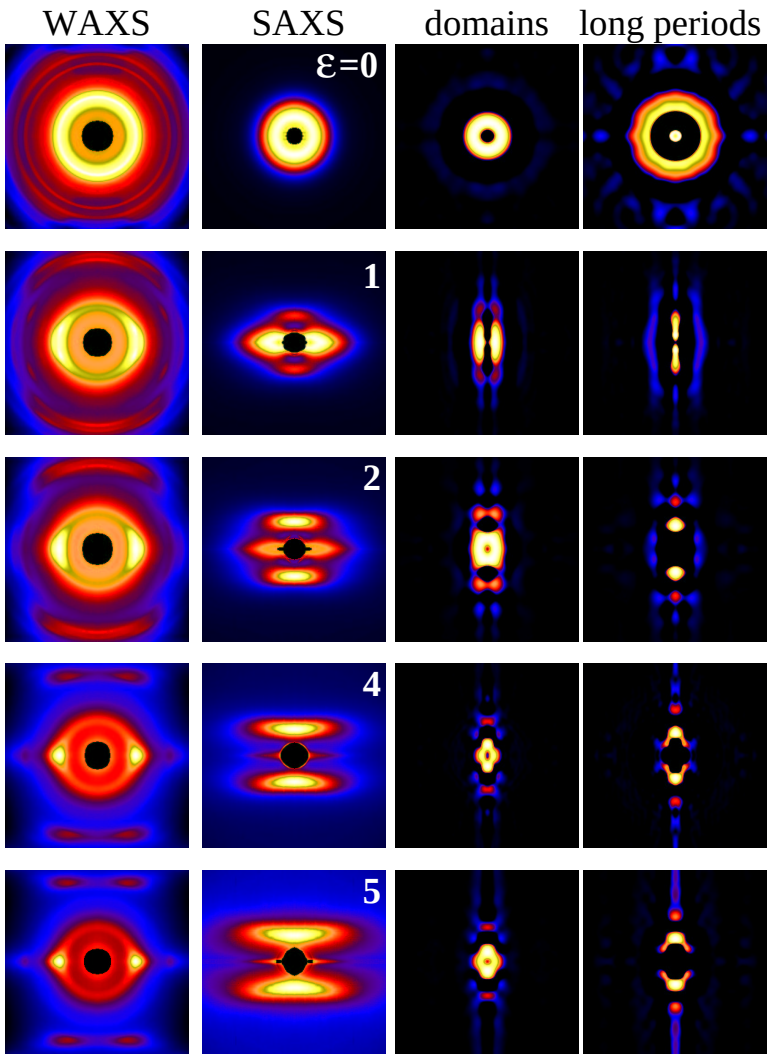

Figure 1: Sample EO19-1. Structure evolution as a function of elongation ε. Straining direction is vertical. Measured data of **WAXS** (logarithmic intensity, region: 12 × 12 cm) and **SAXS** (region: $-0.25\,\mathrm{nm}^{-1} < s_{12},\, s_3 < 0.25\,\mathrm{nm}^{-1}$) are shown on the left hand side. The right hand side displays the CDF (logarithmic intensity; region: $-50\,\mathrm{nm} < r_{12},\, r_3 < 50\,\mathrm{nm}$) computed from the SAXS data. **domains**: Positive peaks revealing the domains of the nanostructure. **long periods**: Negative peaks revealing domain arrangement.

The fourth column shows the negative peaks of the CDF in a logarithmic peak intensity scale. These peaks visualize the distances between domains, i.e. long periods and their multiples. If nanosize domains inside the sample form a distinct lattice those peaks are strong. At low elongations this is not the case for the studied samples. The long period peaks are smaller by one order of magnitude than the domain peaks on the opposite face of the CDF. Thus weak features that show up at low elongations in the fourth column of the images are considered artifacts of the discrete Fourier transformation.

Scattering Data Recorded after Relaxation

Figure 7 shows the final structure of the slowly cooled samples after straining, unloading and waiting for 12 h. The corresponding images of the quenched samples look very similar.

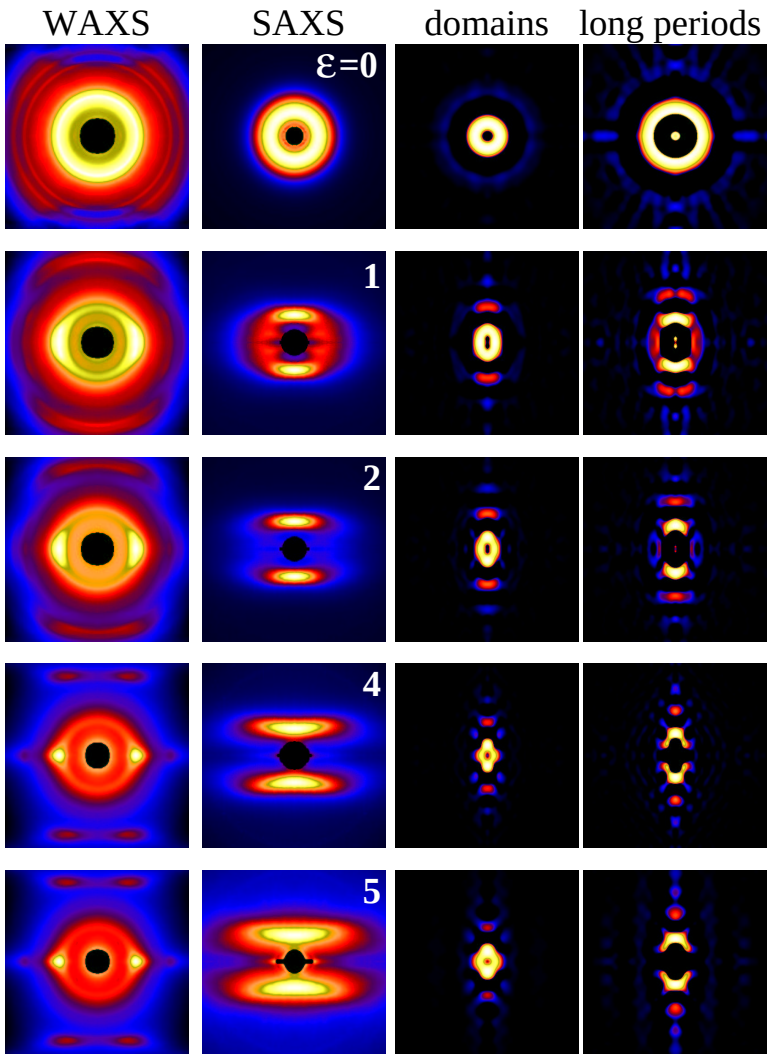

Figure 2: Sample EO19-q. Structure evolution as a function of elongation ε. Measured data of **WAXS** (logarithmic intensity) and **SAXS**. Columns 3 and 4 display the CDF (logarithmic intensity) from the SAXS data. **domains**: Positive peaks revealing the domains of the nanostructure. **long periods**: Negative peaks revealing domain arrangement.

Poly(ethylene-*co*-1-octene) EO19

EO19-1: Slowly Cooled

In Figure 1 at $\varepsilon = 0$ isotropic WAXS and SAXS is observed. Computing the long period from the position of the SAXS maximum (second column) a value of 20 nm is found. Because of the underlying Porod's law this uncorrected value is too big.[23] From the maximum of the CDF (fourth column) a more realistic average of $\bar{L} = 15.3$ nm is obtained. The maximum on the positive face of the CDF (third column) yields an average domain diameter of 7.1 nm. The domain distributions of crystalline and amorphous phases are not separated.

At $\varepsilon = 1$ a detailed SAXS image ('figure-eight pattern' and two meridional spots) is observed that was previously[17] interpreted as stacks of lamellae with their axes oriented mainly perpendicular to the direction of strain. Here the 'axis of a lamellar stack' is defined as established in SAXS theory, where the lamellar stack is a pile of extended, circular discs and its axis passes through the center of each disc. In the third column we now detect the basic domain. The two strong intensity ridges parallel to the meridian are generated from the correlation between the left and the right surface of a constricted layer, i.e. a disc. So their distance from the merid-

ian yields the average disc thickness, i.e. its width in equatorial direction, $\bar{D}_e = 4.1$ nm, and the longitudinal extension of the peak returns a measure of the average lateral extension of the disc (in the meridional direction), $D_m = 11.9$ nm. However, there is no 'stack' of lamellae. Not even a second layer is found to be attached to the side of the representative disc, in contrast to the results of an investigation of the nanostructure from polyether-*block*-polyamide copolymers.[24] Nevertheless, the fourth column shows two weak intensity ridges crossing the equator at a distance of $\bar{L}_e = 13.8$ nm, and this is the nanostructural feature that generates the equatorial maximum of the observed SAXS 'figure-eight'. In order to explain this feature of the nanostructure, let us associate the cross section of the observed crystalline layer by a rectangular island extending from north to south on a map of the earth.

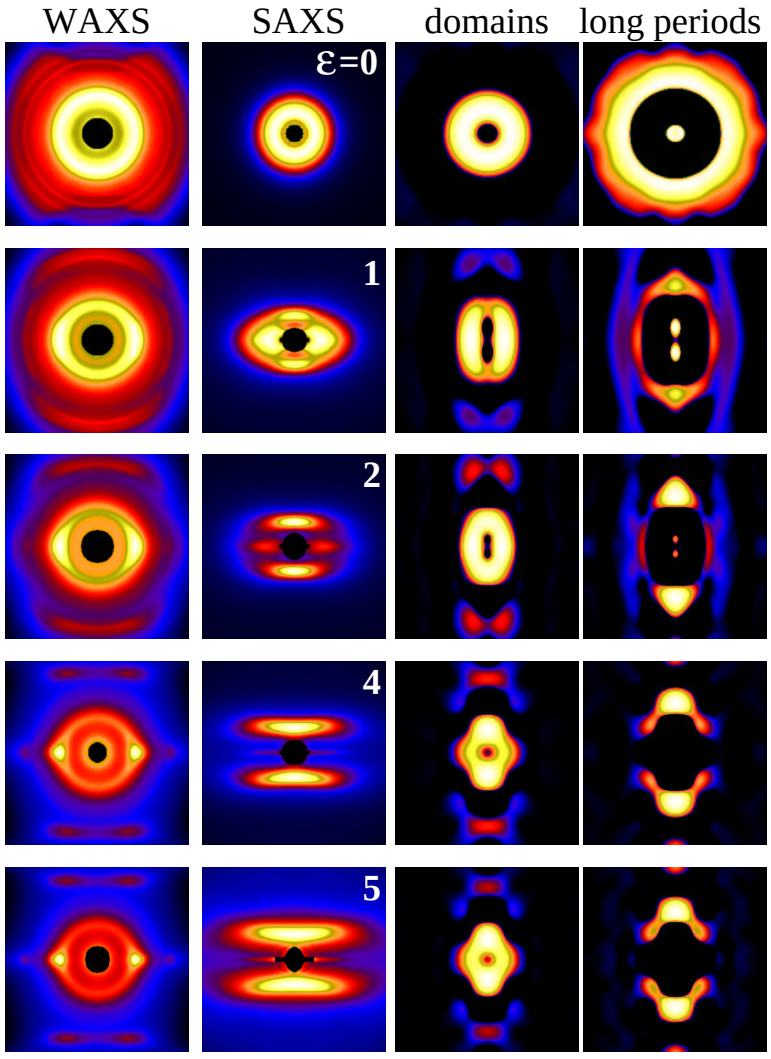

Figure 3: Sample EO30-1. Structure evolution as a function of elongation ε. Measured data of **WAXS** (logarithmic intensity) and **SAXS**. Columns 3 and 4 display the CDF (logarithmic intensity, region: $-25\,\text{nm} < r_{12}, r_3 < 25\,\text{nm}$) from the SAXS data. **domains**: Positive peaks revealing the domains of the nanostructure. **long periods**: Negative peaks revealing domain arrangement.

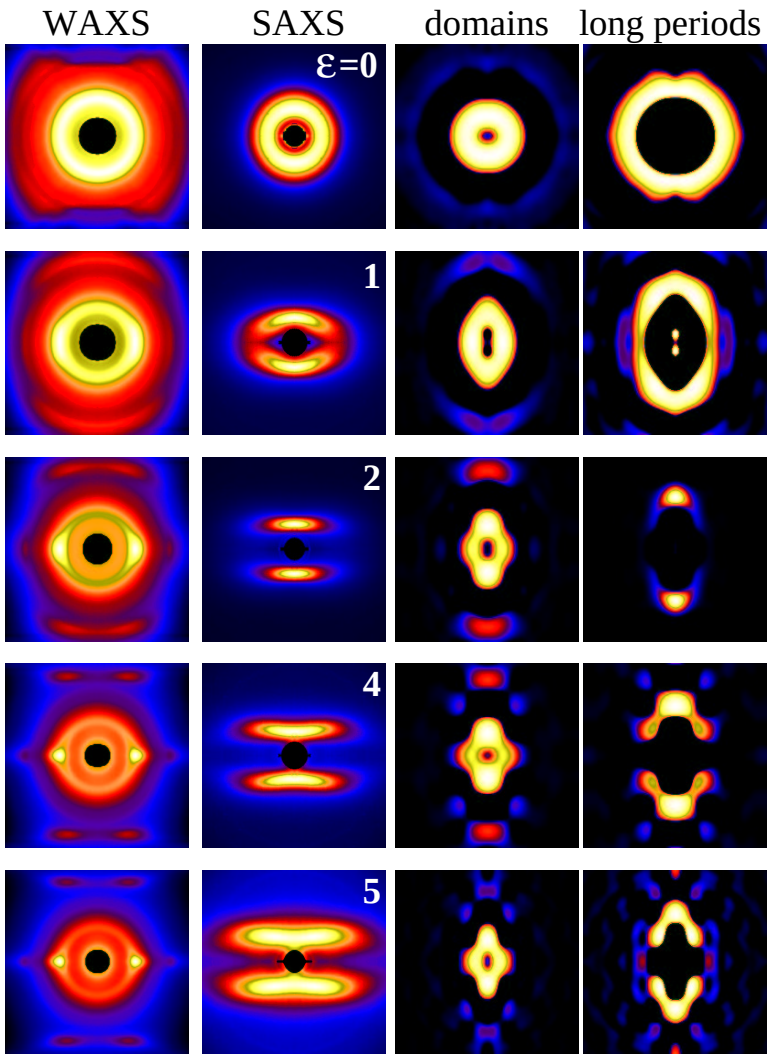

Figure 4: Sample EO30-q. Structure evolution as a function of elongation ε. Measured data of **WAXS** (logarithmic intensity) and **SAXS**. Columns 3 and 4 display the CDF (logarithmic intensity, region: $-25\,\mathrm{nm} < r_{12}, r_3 < 25\,\mathrm{nm}$) from the SAXS data. **domains**: Positive peaks revealing the domains of the nanostructure. **long periods**: Negative peaks revealing domain arrangement.

The CDF then tells us that there is a considerable probability to find a western shore of some other land in a distance of 13.8 nm from the western shore of our island. Nevertheless, nothing is known about the size of the neighboring continent or island. In short, every crystalline lamella is covered by an amorphous border layer, $\bar{a}_e = \bar{L}_e - \bar{d}_e$, of well-defined thickness (here: $\bar{a}_e = 9.7\,\mathrm{nm}$). Such 'stacks made from 1.5 lamellae' were first reported in a study of ethylene copolymers by SAXS in 1974 (Kilian and Wenig[25]). At that time the authors drew their conclusion from a quantitative peak shape analysis of isotropic SAXS data. Moreover, our finding is consistent with the characteristics associated with the 'Type–2' morphology[3] of this polymer (mixed lamellae and bundled crystals).

The strongest peak in the fourth column of Figure 1, at $\varepsilon = 1$, is found on the meridian. It extends in the vertical direction and describes a very wide long period distribution between (fractions of) domains that line up in the direction of strain, indicating the beginning of microfibrillation. A comparison with the stress-strain curves published in previous work,[17] reveals that $\varepsilon = 1$ is close to the second yield point of this sample. Thus the CDF analysis confirms the finding

of the group of Ryan[10] concerning the onset of irreversible microfibrillation.

During the course of further elongation the layers (third column) are destroyed at the expense of a growing microfibrillar structure. The lateral long period (fourth column) weakens and the long period of the microfibrils on the meridian, $\overline{L}_m$, becomes stronger. The central domain peak (third column) moves towards the center and changes its shape, at $\varepsilon = 4$ showing the characteristics of perfectly oriented cylindrical domains with a rather narrow distribution of heights and diameters. At higher elongation the peak, again, broadens demonstrating the broadening of the domain size distribution. On the long period face (fourth column) more and more orders can be detected in the microfibrillar arrangement. Moreover, at $\varepsilon = 4$ two 'tentacles' have emerged from each of the main long period peaks and indicate emerging lateral order among the domains from neighboring microfibrils. At the same time the main peak has narrowed showing increased perfection of the lattice constant in the irradiated volume. Some of this perfection gets lost upon further straining.

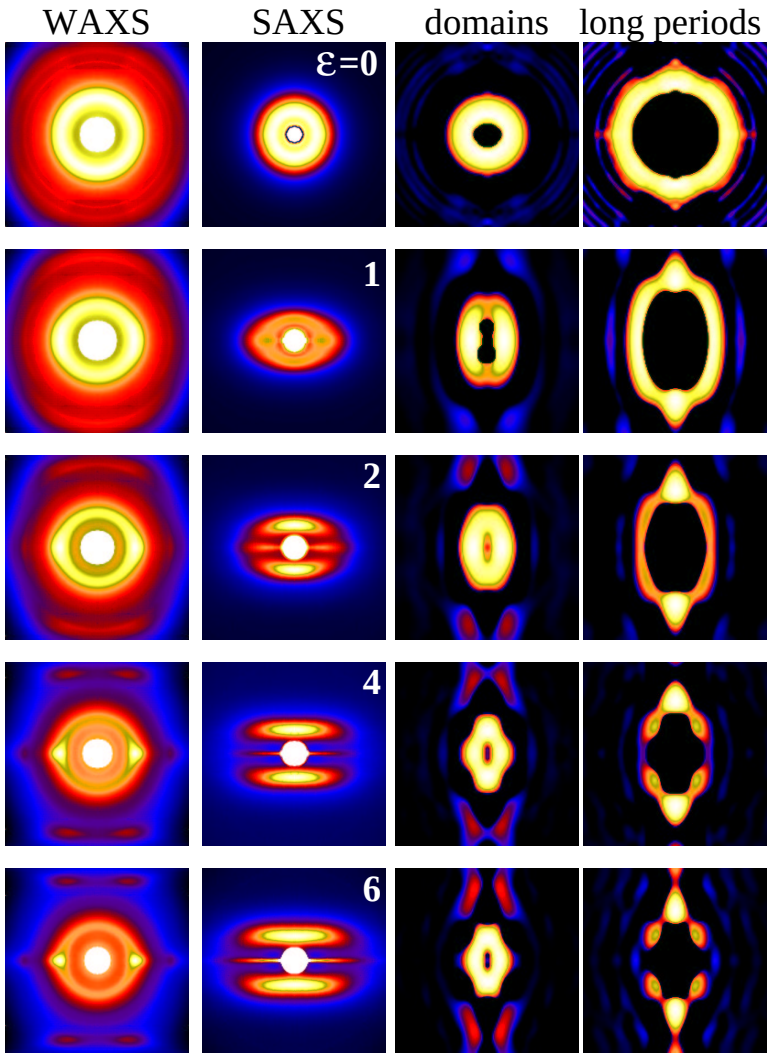

Figure 5: Sample EO38-1. Structure evolution as a function of elongation ε. Measured data of **WAXS** (logarithmic intensity) and **SAXS**. Columns 3 and 4 display the CDF (logarithmic intensity, region: $-25\,\text{nm} < r_{12}, r_3 < 25\,\text{nm}$) from the SAXS data. **domains**: Positive peaks revealing the domains of the nanostructure. **long periods**: Negative peaks revealing domain arrangement.

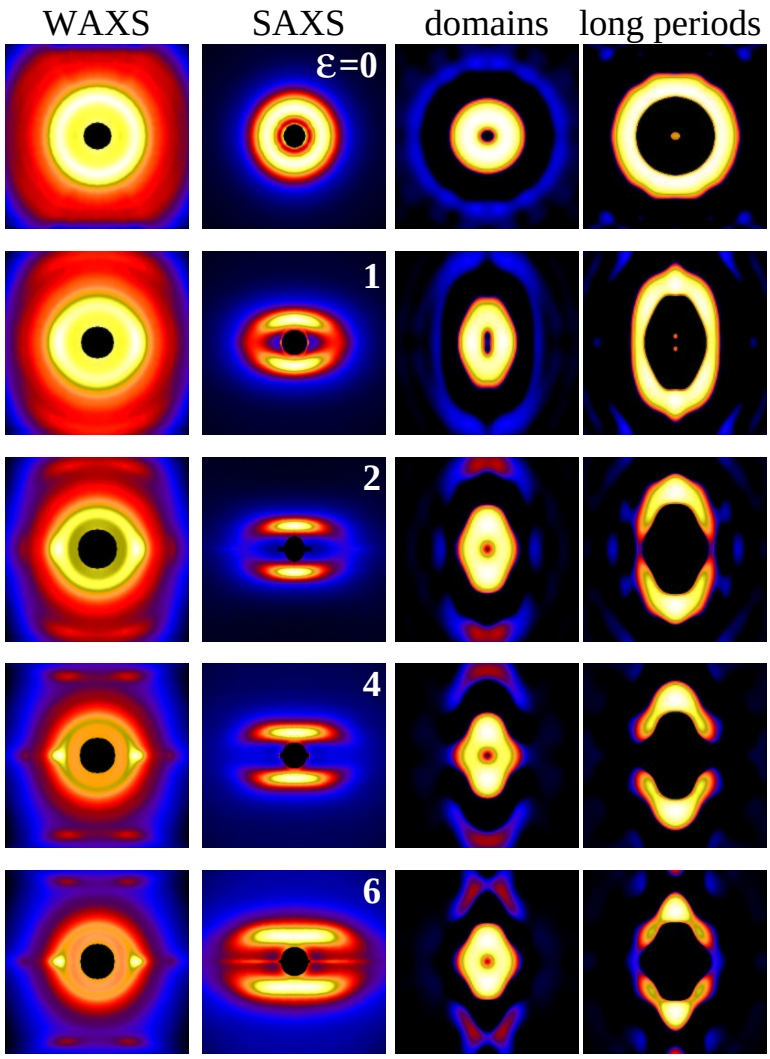

Figure 6: Sample EO38-q. Structure evolution as a function of elongation ε. Measured data of **WAXS** (logarithmic intensity) and **SAXS**. Columns 3 and 4 display the CDF (logarithmic intensity, region: $-25\,\text{nm} < r_{12}, r_3 < 25\,\text{nm}$) from the SAXS data. **domains**: Positive peaks revealing the domains of the nanostructure. **long periods**: Negative peaks revealing domain arrangement.

EO19-q: Quenched

The quenched sample (Figure 2) exhibits an almost identical series of WAXS patterns as a function of strain. On the other hand, the SAXS series differ from each other. In the isotropic state the CDF yields a long period of $\bar{L} = 13.6\,\text{nm}$, a value considerably smaller than that found in the slowly cooled sample. At $\varepsilon = 1$ the CDF shows no lamellae (third column). The majority of crystals are granular ones. They arrange (fourth column) in microfibrillar structures with a peculiar inclination of 7^{o} with respect to the draw direction.

Upon further strain the difference between the slowly cooled and the quenched material becomes smaller. The microfibrils become perfectly oriented and the rest of the sequence shows similar features of lateral arrangement as the slowly cooled material. In the ultimate nanostructure the main difference between both samples is an increased lateral distance between neighboring microfibrils in the quenched sample.

In summary, the CDF shows that moderate straining has erased differences concerning the thermal history except for the seeded number of the crystals per volume. Moreover, it

has improved the arrangement of the crystallites and has harmonized crystallite size and shape. At high strain, again, the distributions of crystallite size and long periods are broadened.

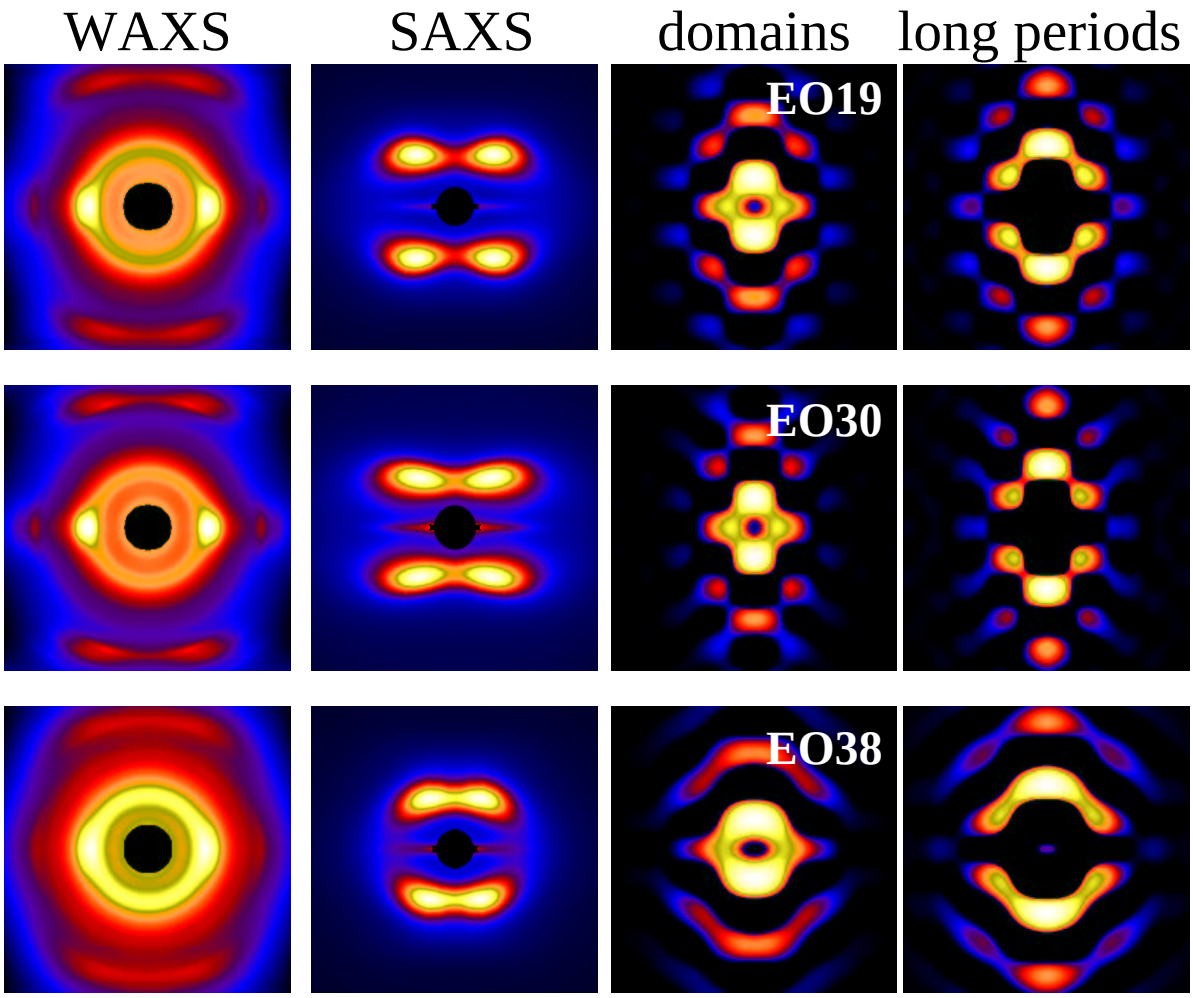

Figure 7: Ethylene-octene Copolymers. Final structure after straining to $\varepsilon = 6$ and relaxation for 12 h as a function of increasing 1-octene content (from top to bottom). Slowly cooled material. Measured data of **WAXS** (logarithmic intensity) and **SAXS**. Columns 3 and 4 display the CDF (logarithmic intensity, region: $-25\,\text{nm} < r_{12}, r_3 < 25\,\text{nm}$) from the SAXS data. **domains**: Positive peaks revealing the domains of the nanostructure. **long periods**: Negative peaks revealing domain arrangement.

Poly(ethylene-*co*-1-octene) EO30

EO30-1: Slowly Cooled

Figure 3 presents recorded data and CDFs of the slowly crystallized sample with a medium content of 1-octene. At $\varepsilon = 0$ isotropic WAXS and SAXS is observed. From the maximum of the SAXS peak a long period of 17 nm is read. The more appropriate average from the CDF is $\bar{L} = 14\,\text{nm}$. Similar to the respective sample with the lowest octene content at $\varepsilon = 1$, the combined scattering pattern of misoriented, standing lamellae ('figure-eight pattern') and microfibrils in their initial state ('layer-line pattern' on the meridian) are observed.

The CDF (third column) shows shape and orientation of the lamellae directly. Concerning the size of the disc-like lamellae we obtain $\bar{D}_e = 4.6\,\text{nm}$ for the thickness and

$D_m = 12.2$ nm for the diameter.

Consulting the long period face of the CDF (fourth column) we find two ridges on each side of the meridian that are associated with the coverage of a layer by an amorphous zone ($\bar{L}_{e,1} = 10.1$ nm and $\bar{L}_{e,2} = 14.5$ nm). This can be explained by a bimodal distribution of cover layers with average thicknesses of $\bar{a}_{e,1} = 5.5$ nm and $\bar{a}_{e,2} = 9.9$ nm.

At higher elongations, again, first the evolution of a microfibrillar system and thereafter of lateral correlation is observed.

EO30-q: Quenched

The isotropic sample (Figure 4) shows a CDF long period of $\bar{L} = 12$ nm. As compared to the slowly cooled material, even the quenched material does not exhibit strong scattering from lamellae at $\varepsilon = 1$. However, the highest long-range order of all the studied samples is achieved in the course of the evolution of the microfibrillar system. We speculate that this might be related to an extremely effective quenching of this sample resulting in very similar crystallite sizes due to suppression of secondary crystallization that is going along with broadening of the crystallite size distributions.

This speculation is supported by the observation of very narrow crystallite size distributions as compared to the other samples. In the ultimate structure the lateral size of the domains inside the quenched material is smaller than that inside the slowly cooled sample.

Poly(ethylene-*co*-1-octene) EO38

EO38-1: Slowly Cooled

For the slowly cooled sample, with the lowest crystallinity, Figure 5 reports the results of the scattering experiments in pseudo color. The SAXS shows the transition from an almost isotropic scattering at $\varepsilon = 0$ to a layer line pattern. In contrast to the materials with lower comonomer content, an extremely narrow equatorial streak is emerging during the course of the straining experiment. At an elongation of $\varepsilon = 2$ it separates from the layer lines, but shows a fanning-out[26,27] which indicates the imperfect orientation of very long (> 200 nm) and thin (5 nm) voids. The values for the dimensions are estimated from the height and the lateral extension of the streak in the SAXS patterns, respectively. Because of its restriction to low spatial frequency in the meridional direction, the nanostructural effect of the voids does not pass the spatial frequency filter as long as we transform the whole scattering pattern. Thus it cannot be observed in our CDFs.

Before the start of the draw experiments the CDF (third column) exhibits a strong domain ring corresponding to an average domain cross section of 5.6 nm. From the CDF a long period of 14 nm is extracted. The SAXS patterns yields 17 nm.

Only up to an elongation of $\varepsilon = 1.5$ the strong, ridge-shaped domain peaks (third column) from constricted lamellae parallel to the straining direction are observed on both sides of the meridian. Disc thicknesses, $\bar{D}_e$, and diameter, D_m, are reported in Figure 8.

In a similar manner on the long period face (fourth column), distinct intensity ridges are crossing the equator on each side of the meridian. Moreover, on the meridian the narrow long period peaks of an emerging microfibrillar component are observed.

Beginning from an elongation of $\varepsilon = 3$, the microfibrillar component can as well be observed on the domain face. Upon further elongation the corresponding domain peak (third column) is gaining strength. Its triangle shaped intensity profile is rather narrow and indicates cylindrical domains with their axes parallel to the draw direction. Concerning the long periods on the meridian three orders of clear maxima are observed (not all visible in the cutouts presented in Figure 5). During the straining from $\varepsilon = 2$ to $\varepsilon = 6$ the intensity ridges (forth column) split and, finally, form a four-point pattern related to moderate lateral correlations among adjacent microfibrils.

EO38-q: Quenched

The structure evolution in the quenched sample with the highest comonomer content is presented in Figure 6. WAXS, SAXS and the CDF exhibit that, obviously, the organization of the scattering entities (lamellae and microfibrils of crystallites) and the homogeneity of their sizes is rather low. The equatorial streak is observed at high elongation only. The other features concerning the nanostructure of this sample are similar to those of EO38-1.

Generalization of the Findings

The Domains

The evolution of domain shape and size as a function of strain is shown in Figure 8 for the sample EO38-1. The figure is in several respects representative for all samples. Up to the appearance of the meridional peak on the domain face of the CDF, predominantly discs are observed. Beginning from a critical elongation, ε_c, mainly cylindrical domains are found that are arranged in microfibrils. Of course, both these domain shapes are simplifications. Deviations from these simplified shapes cannot be extracted from the SAXS patterns because of the considerable variation of domain sizes in the volume irradiated by the synchrotron beam, that has to be

considered in any quantitative analysis. As a function of increasing strain the lower limit for the disc diameters, D_m, is decreasing from 12.5 nm to 10 nm. This effect is hardly overestimated even if the determination of D_m from the zero of the function is rather uncertain, because the orientation of the discs increases at the same time.

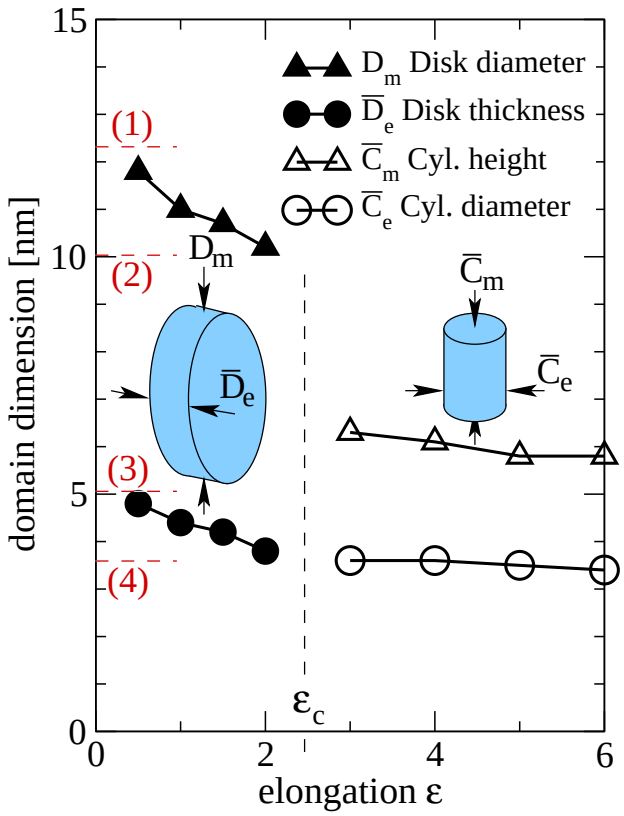

Figure 8: EO38-1 (slowly cooled). Evolution of shape and size of the nanodomains as a function of elongation. Acceleration of the cooling shifts ε_c to lower values. Constant are the initial disc diameter (1), the diameter at the critical elongation (2), the initial disc thickness (3), and the disc thickness at ε_c (4).

Similarly, the average disc thickness, $\bar{D}_e$, is decreasing. It is determined from the position of the intensity maximum on the equator of the CDF. After crossing the critical elongation, shape and position of the domain peaks remain almost constant. Cylindrical domains of 6 nm height and less than 4 nm diameter are observed.

In the same manner we have plotted the data of all samples and of a material EO38-10 (not mentioned up to now) that was cooled at an intermediate rate of 10 K/min. The corresponding plots look very similar. e_c shifts with increasing cooling rate to smaller values ($\varepsilon_c \approx 1.7$ and $\varepsilon_c \approx 1.2$ for 10 K/min and the quenched material, respectively), and we speculate that the most probable reason is an increase of defects in the lamellae with increasing cooling rate. Constant remain the ranges concerning D_m and $\bar{D}_e$ that are traversed (in a melt-off process) by all disc shaped domains before they fail.

As a function of comonomer content both crystallinity and the number of lamellae per volume are decreasing. We observe that ε_c is increasing from $\varepsilon_c \approx 1.5$ for EO19-1 to a value of $\varepsilon_c \approx 2.5$ for EO38-1 (cf. Figure 8). This can be explained by the additional degrees of freedom in the samples with a low concentration of lamellae, that allow for a considerable macroscopic straining without early accumulation of sufficient local stress to disrupt the lamellae.

Thus in the multidimensional CDF from SAXS patterns the impact of 'fine chain slip'[10] on shape and size of the crystalline domains is directly observed during the draw experiment. At ε_c 'coarse chain slip'[6,7,10,28] is initiated and the domains are transformed into fragments of rather uniform size that does not change any more up to the highest strain of the experiments.

The Long Periods

As soon as a pointed long period reflection is observed on the meridian of the CDF, microfibrils are present. The position of this peak, $\bar{L}_m$, is related to the most probable long period of these microfibrils. Figure 9 shows $\bar{L}_m$ as a function of comonomer content, thermal pretreatment and strain of the samples.

Obviously the microfibrillar long period is decreasing as a function of decreasing comonomer content. The thermal treatment has no significant effect on the long period, whereas a considerable decrease of $\bar{L}_m$ is observed as a function of elongation.

Initially and with increasing elongation, the intensity of the long period peak in the CDF is increasing. In the (r_{12}, r_3)-plane it covers a triangular area: the narrowest microfibrils show the longest long periods. The long period distribution is wide and covers values in an interval from 11 nm to 18 nm at least.

Beginning from $\varepsilon = 3$ all samples start to show lateral correlations among neighboring microfibrils (macro lattice with short-range correlation, cf. [29]). The long period distribution is narrowed and the average value generally diminished. Then, for $\varepsilon > 3$ the peak becomes wider, again. Now the peak covers a rectangular area in the (r_{12}, r_3)-plane, showing that there is no correlation between individual long period and diameter of the microfibril any more. Narrow microfibrils with a long repeat have vanished.

From this observation an explanation for the observed further decrease of the long period with increasing strain is obvi-

ous: Similar to the initial destruction of the narrow microfibrils with a long repeat, continued preferential destruction of the microfibrils with the longest long periods is likely to happen. Thus, despite further increase of the macroscopic strain, the average long period of the remnant microfibrils is decreasing. Another possibility for an observed decrease of the long period would be the insertion of new crystals by stress-induced crystallization in the microfibrils. In order to discriminate between the two possibilities, it would have been necessary to carry out the SAXS measurements on an absolute scale and then to analyze the patterns quantitatively. A viable route would start from computing the longitudinal scattering curve[30] from the 2D pattern and then to fit it using one-dimensional paracrystalline stacking models, as has been published earlier.[31, 32] Crystallinity in the microfibrils could be approximated from the analysis of the longitudinal structure as well. Using information already gathered in our present multidimensional study we could even compute the total volume crystallinity under some not very restrictive assumptions.

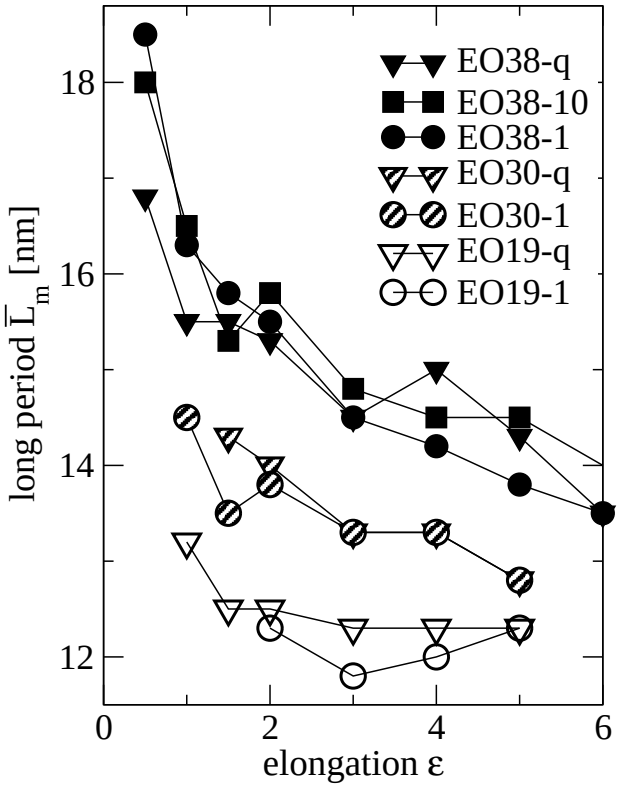

Figure 9: Most probable microfibrillar long period, $\bar{L}_m$, in ethylene-octene copolymers as a function of 1-octene content (38, 30, 19 wt.-%) and of thermal pretreatment (quenched from the melt, cooled at 10 and 1 K/min).

The General Features of Nanostructure Evolution

In summary, the nanostructure evolution during the homogeneous straining of the studied ethylene-octene copolymers can be described as follows:

1. In the initial colloidal structure there are granular crystallites. If lamellae are present, their lateral extension is finite ('discs'), and they are covered by amorphous layers of well-defined thickness. Beyond that there is no organization of layers in stacks of lamellae. The faster the melt has been cooled, the lower is the content of lamellae and the more uniform are the domains.

2. At low strain, domains are oriented and at the same time 'fine chain slip' melts off the domains. Even at this low elongation granular crystallites start to line up resulting in entities that are carrying all the topological features of microfibrils (i.e. alternating hard and soft domains within a rod that is oriented parallel to the draw direction). Discoidal crystallites rotate to finally orient their planes parallel to the draw direction.

3. Microfibrillation (coarse chain slip) destroys the discoidal crystals and, in combination with fine chain slip, results in uniform domain sizes. Now most of the thermal history of the sample is erased, except for the seeded number of crystallites per volume and some remnant variation of their sizes.

4. From the microfibrils populated by uniform domains, oriented macrolattices with short-range correlation[29] are formed.

5. At higher elongation, in the regime of strain hardening,[4, 12, 33] the averaged nanostructure is blurred from inhomogeneous tension.[9, 34] The microfibrils that are most widely strained fail first, resulting in the observed decrease of the most probable long period as a function of increasing strain.

The Different Materials and their Ultimate Nanostructures

All the ultimate structures are highly oriented, observed both by WAXS and SAXS. With increasing comonomer content the range of the longitudinal correlation among the crystallites inside a microfibril is decreasing. The two materials with the lower comonomer content (EO19 and EO30) generate macrolattices with rather uniform domain sizes and distances. The perfection and the lateral extension of the lattices is highest when the original film was quenched from the melt.

For EO38 the peaks of the CDF are considerably blurred. Thus domain sizes and distances are less uniform than in the colloidal structure of the other materials. This polydispersity is widest in the quenched sample, i.e. the specimen with the initially lowest amount of lamellae.

Final Structures in the Relaxed State

The final structures after relaxation of 12 h are presented in Figure 7. All the patterns originate from slowly cooled samples. The patterns of the quenched samples are not shown because of their similarity. Compared to the nanostructure in the strained state, the peaks in the CDFs of relaxed EO19 and EO30 are much narrower. Bearing in mind the observation of strain broadening at high elongations, this finding can be explained by the effect of unloading the macroscopical stress to the distribution of local tensions in the irradiated volume. Inhomogeneity of tension on the nanometer scale is removed, allowing for a perfecting of the macrolattices.

The final structure of EO38 is different. Not only is the ultimate structure at high elongation much less perfect as for the other samples, but also shows the final relaxed nanostructure some orientation relaxation. We ascribe this quasi-elastic behavior to the fact that a sufficient number of stabilizing fragments of lamellae is missing.

Compared to the ultimate nanostructure at high elongation, the WAXS reflections generally appear to be subject to some moderate orientation relaxation, even for EO19 and EO30 that show perfectly oriented macrolattices in the relaxed state.

For all the materials the shape of the crystallites is not lamellar but can be approximated by cylinders with an average height, $\bar{C}_m$, close to 5 nm. The domain diameter, $\bar{C}_e$, has grown and returned to range from 4.1 nm to 4.5 nm. Thus CDF analysis confirms that fine chain slip is a reversible process.[10]

The most probable long period of the microfibrils, $\bar{L}_m$, is 10.6 nm for EO19 and EO30-1. EO30-q and EO38 yield 11.1 nm. A discussion appears to be inappropriate because of the narrow basis of our data.

The closest domain from the adjacent microfibril is always found at an angle between 46^{o} and 51^{o}, as measured with respect to the meridian. The distance is increasing with increasing comonomer fraction from 7.7 nm to 9.4 nm in the slowly cooled samples. In the quenched samples it is somewhat longer (8.1 nm to 10 nm). This finding is plausible, because the number of crystallites per sample volume is decreasing both as a function of increasing comonomer fraction and cooling rate.

Comparison of CDF Interpretation with Direct Interpretation of the SAXS

In a preceding study[17] we have interpreted part of the SAXS data directly and have drawn different conclusions than those presented here from the interpretation of the CDF. Considering the scope of a SAXS interpretation and comparing it to the possibilities of CDF analysis, the alleged contradictions are resolved. Similar comparison has been published some time ago[23] for the case of nanostructure extraction directly from SAXS curves, from the linear correlation function, and from the interface distribution function.

The CDF exhibits that the long period in a polymer sample is subject to considerable variation. If the long period is determined directly from the maximum of the peak in the SAXS pattern, it is found on the background of Porod's law falling off with s^{-4}. The observed maximum thus reflects the inner edge of the long period distribution in reciprocal space, i.e. the outer edge of the distribution in physical space. Thus from the SAXS not an average, but the upper limit is determined. Bearing in mind the results of this study, the 'SAXS average' corresponds to the long periods of those microfibrils failing just now. This 'breakaway long period' can be determined from the CDF as well. An estimate is obtained from the position of the outward zero of the peak that is found to be at about 18 nm for all samples. More precise specifications can only be given after separation of the overlapping peaks of the CDF.

The long period $\bar{L}_m$ reported in this work is related to the value found with most of the microfibrils. Here, as well, only an estimate is reported, as long as the distributions themselves are not separated.

From the direct analysis of the SAXS we have concluded that microfibrillation is shifting to shorter elongation as a function of increasing comonomer fraction. Here we find that ε_c shifts to higher values, and ε_c is the elongation at which the lamellae are disrupted and form microfibrils. As well, this is a contradiction only at the first glance. Our more elaborate study shows that the investigated specimens contain both granular crystallites and lamellae. Moreover, the granular crystallites can be arranged one upon the other (stringed) by moderate drawing. This effect is sufficient to generate the layer line pattern of the SAXS that in the preceding study was taken to indicate microfibrils. And in fact, the stringed granules meet the geometrical definition of a microfibril: A periodical sequence of crystalline and amorphous zones constricted to a virtual rod that is oriented parallel to the draw direction.

The CDF separates the peaks of the lamellae from those of the granules, and for the first time we can directly observe the disruption of the lamellae at ε_c. It should be obvious that

lamellae diluted in a granular environment behave different than lamellae from a lamellar system, in which the required stress for disruption is attained at lower strain.

Thus the observation of a second yield point in the stress-strain plot is, for ethylene-octene copolymers, a sufficient criterion for the activation of coarse chain slip,[10] but not a necessary one. Insofar our data support the result of the group of Ryan, and our results extend it for the case of ethylene-octene copolymers with a high comonomer content.

Conclusions

In our investigation of the nanostructure evolution of ethylene-octene copolymers with low crystallinity we have utilized both the advanced facilities of synchrotron radiation and used the novel method of multidimensional CDF analysis. Thus we have extracted quantitative structural parameters and gained insight into the underlying processes. Moreover, the visualization of the CDF as a function of strain demonstrates how these processes are intertwined. These processes are stringing of granular crystallites in the draw direction, lamella rotation, crystallite thinning, loading of the strings with a stress distribution, fracture of lamellae, the classical microfibrillation from fragments, equalization of domain sizes by fine chain slip, the formation of lateral order among microfibrils (macrolattice) and the loading of this lattice with a stress distribution. If the original specimen contained a sufficiently high fraction of crystalline lamellae the subsequent relaxation and the corresponding cancellation of stress cause further improvement of regularity in the ensemble of colloidal lattices without loss of orientation.

At the end of this investigation several questions arise. What is the stabilizing effect of the broken lamellae? Is there a method to grow even bigger colloidal crystals from the evidential nuclei with short range order? Intertwined cycles of thermal and mechanical load might be worth the investigation in the synchrotron beam.

Acknowledgments. The authors thank the Dow Chemical Co. for providing the samples. Support for this study by HASYLAB, Hamburg, Project II-01-041, is gratefully acknowledged.

References

[1] A. Prasad, in: J. E. Mark, Ed. 'Polymer Data Handbook', Oxford University Press, Oxford, **1999** pp. 529–539.
[2] N. Stribeck, *J. Appl. Cryst.* **2001**, *34*, 496.
[3] S. Bensason, J. Minick, A. Moet, S. Chum, A. Hiltner, E. Baer, *J. Polym. Sci. Part B: Polym. Phys.* **1996**, *34*, 1301.
[4] H. Y. Chen, S. P. Chum, A. Hiltner, E. Baer, *J. Polym. Sci. Part B: Polym. Phys.* **2001**, *39*, 1578.
[5] A. Chang, Y. W. Cheung, A. Hiltner, E. Baer, *J. Polym. Sci. Part B: Polym. Phys.* **2002**, *40*, 142.
[6] A. Peterlin, *Text. Res. J.* **1972**, *42*, 20.
[7] A. Peterlin, *J. Mater. Sci.* **1971**, *6*, 490.
[8] F. J. Baltá Calleja, *Adv. Polym. Sci.* **1985**, *66*, 117.
[9] R. Bonart, F. Bötzl, J. Schmid, *Makromol. Chem.* **1987**, *188*, 907.
[10] M. F. Butler, A. M. Donald, A. J. Ryan, *Polymer* **1997**, *38*, 5521.
[11] M. F. Butler, A. M. Donald, *Macromolecules* **1998**, *31*, 6234.
[12] M. F. Butler, A. M. Donald, A. J. Ryan, *Polymer* **1998**, *39*, 781.
[13] A. D. Drozdov, A. Dorfmann, *Comput. Mater. Sci.* **2001**, *21*, 395.
[14] M.-C. G. Jones, D. C. Martin, *Macromolecules* **1995**, *28*, 6161.
[15] M. F. Butler, A. M. Donald, W. Bras, G. R. Mant, G. E. Derbyshire, A. J. Ryan, *Macromolecules* **1995**, *28*, 6383.
[16] R. Androsch, J. Blackwell, S. N. Chvalun, B. Wunderlich, *Macromolecules* **1999**, *32*, 3735.
[17] R. Androsch, N. Stribeck, T. Lüpke, S. Funari, *J. Polym. Sci. Part B: Polym. Phys.* **2002**, *40*, 1919.
[18] N. Stribeck, *Colloid Polym. Sci.* **2002**, *280*, 254.
[19] M. D. Buhmann, *Acta Numerica* **2000**, *9*, 1.
[20] C. G. Vonk, *Colloid Polym. Sci.* **1979**, *257*, 1021.
[21] W. Ruland, *Colloid Polym. Sci.* **1977**, *255*, 417.
[22] W. Ruland, *Colloid Polym. Sci.* **1978**, *256*, 932.
[23] C. Santa Cruz, N. Stribeck, H. G. Zachmann, F. J. Baltá Calleja, *Macromolecules* **1991**, *24*, 5980.
[24] V. Barbi, S. S. Funari, R. Gehrke, N. Scharnagl, N. Stribeck, *Macromolecules* **2003**, *38*, 749.
[25] H. G. Kilian, W. Wenig, *J. Macromol. Sci. - Phys.* **1974**, *B9*, 463.
[26] W. Ruland, *J. Polym. Sci., Part B: Polym. Phys.* **1969**, *28*, 143.
[27] A. F. Thünemann, W. Ruland, *Macromolecules* **2000**, *33*, 1848.
[28] A. Cowking, J. G. Rider, *J. Mater. Sci.* **1969**, *4*, 1051.
[29] W. Fronk, W. Wilke, *Colloid Polym. Sci.* **1985**, *263*, 97.
[30] R. Bonart, *Kolloid Z. u. Z. Polymere* **1966**, *211*, 14.
[31] N. Stribeck, S. Fakirov, D. Sapoundjieva, *Macromolecules* **1999**, *32*, 3368.
[32] Z. Wang, B. S. Hsiao, N. Stribeck, R. Gehrke, *Macromolecules* **2002**, *35*, 2200.
[33] M. A. Kennedy, A. J. Peacock, M. D. Failla, J. C. Lucas, L. Mandelkern, *Macromolecules* **1995**, *28*, 1407.
[34] U. Dehlinger, A. Kochendörfer, *Z. Kristallograf.* **1939**, *101*, 134.